An implementation of the v^2-f model with application to transonic flows

By Georgi Kalitzin

1. Motivation and objectives

This report describes the implementation of the v^2-f model in CFL3D, a code which solves the time-dependent 3-D compressible Reynolds-averaged Navier-Stokes equations using multi-block structured grids.

The turbulence transport equations are solved implicitly with an implicit treatment of the boundary conditions. The large amount of computer memory required for inversion of the matrices resulting from the implicit operator with, for example, GMRES is still a major constraint for computations of 3-D flow around complex geometries. A three-factored Approximate Factorization scheme, which factorizes the 3-D matrix into three 1-D matrices, minimizes the memory required. The stiffness of the ϵ and f boundary conditions require that the source terms and boundary conditions are treated implicitly in the factorized matrix for grid lines normal to the wall. This, however, leads to severe difficulties in the computation of, for example, wing-body junctions, where grid lines of two coordinate directions may be normal to the walls.

A two-factored Approximate Factorization scheme, which factorizes the 3-D matrix into a 2-D and a 1-D matrix, improves the robustness and applicability of the model. The factorization errors scale with Δt^2 in this scheme in contrast to Δt^3 in the three-factored scheme for 3-D flows. GMRES is used for the inversion of the 2-D matrix, and a direct solver is used for the inversion of the 1-D matrix.

The correctness of the implementation of the v^2-f model in CFL3D has been tested on several cases: flow over a flat plate, channel flow, and by-pass transition. Results for the channel flow have been included in this report.

The performance of each numerical scheme has been tested on the computation of transonic flow around the ONERA M6 wing. This 3-D single block test case presented no major numerical problems with any of these schemes, and it allows a quick evaluation of the CPU time and memory requirements of the different numerical methods. The pressure distributions computed on selected wing cuts are compared with experimental data. Comparisons to computations with the Spalart-Allmaras model provide an overall view on the relative cost of computation for the v^2-f model.

2. Accomplishments

2.1 Basic numerical method

CFL3D, a code developed at NASA (Krist *et al.* 1997), solves the time-dependent thin-layer Reynolds-averaged Navier Stokes equations using multi-block structured

grids. A semi-discrete finite-volume approach is used for the spatial discretization. The convective and diffusion terms are discretized with a third-order upwind and a central difference stencil, respectively. The code uses flux-difference splitting based on the Roe-scheme with a smooth flux limiter. Time advancement is implicit. A three-factored Approximate Factorization scheme (Beam and Warming 1978) is used to invert the matrices, resulting from the implicit operator. The steady-state computations have been performed by marching in time from an initial guess. To accelerate convergence, local timestepping is used for all variables both mean flow and turbulence, while multigrid is used only for the mean flow. This code is a state-of-the art flow solver which is widely used at NASA for research and in industry for design purposes.

2.2 Durbin's v^2-f turbulence model

A short description of the model's equations is given to facilitate the description of its implementation in CFL3D. While new versions of the model (Lien *et al.* 1996, 1998) have been developed to overcome some of the numerical problems mainly connected with the f-boundary condition, we consider in this report only the original version of the model. For high Reynolds number flows in particular the original version predicts consistently better skin friction distributions.

In essence the v^2-f model introduced by Durbin (1995) extends the standard k-ϵ model to low-Reynolds number flow regions. This is realized by modifying the eddy-viscosity formulation and solving two additional partial differential equations: an equation describing the transport of the turbulent intensity normal to the streamlines $\overline{v^2}$ and an elliptic relaxation equation for f. The latter models the effect of the pressure-strain term.

Consistent with the non-dimensionalization used in the code

$$k=\frac{\tilde{k}}{\tilde{a}_\infty^2},\ \epsilon=\frac{\tilde{\epsilon}\tilde{\nu}_\infty}{\tilde{a}_\infty^4},\ \overline{v^2}=\frac{\tilde{\overline{v^2}}}{\tilde{a}_\infty^2},\ f=\frac{\tilde{f}\tilde{\nu}_\infty}{\tilde{a}_\infty^2},\ \mu=\frac{\tilde{\mu}}{\tilde{\mu}_\infty},\ \rho=\frac{\tilde{\rho}}{\tilde{\rho}_\infty},\ U=\frac{\tilde{U}}{\tilde{a}_\infty},\ x=\frac{\tilde{x}}{\tilde{L}_R},\ t=\frac{\tilde{t}\tilde{a}_\infty}{\tilde{L}_R}$$

the model's equations for compressible flow are:

$$\partial_t k=\left(\frac{M_\infty}{Re}\right)\frac{1}{\rho}\nabla\cdot\left[(\mu+\frac{\mu_t}{\sigma_k})\nabla k\right]-U\cdot\nabla k+\left(\frac{M_\infty}{Re}\right)P_k-\left(\frac{Re}{M_\infty}\right)\epsilon \quad (1)$$

$$\partial_t \epsilon=\left(\frac{M_\infty}{Re}\right)\frac{1}{\rho}\nabla\cdot\left[(\mu+\frac{\mu_t}{\sigma_\epsilon})\nabla \epsilon\right]-U\cdot\nabla\epsilon+\left(\frac{M_\infty}{Re}\right)\frac{C_{\epsilon 1}P_k}{T}-\left(\frac{Re}{M_\infty}\right)\frac{C_{\epsilon 2}\epsilon}{T} \quad (2)$$

$$\partial_t \overline{v^2}=\left(\frac{M_\infty}{Re}\right)\frac{1}{\rho}\nabla\cdot\left[(\mu+\frac{\mu_t}{\sigma_k})\nabla \overline{v^2}\right]-U\cdot\nabla\overline{v^2}+\left(\frac{Re}{M_\infty}\right)kf-\left(\frac{Re}{M_\infty}\right)\frac{\epsilon}{k}\overline{v^2} \quad (3)$$

$$0=\left(\frac{M_\infty}{Re}\right)^2 L^2\nabla^2 f-f+\frac{C_1}{T}\left[\frac{2}{3}-\frac{\overline{v^2}}{k}\right]+\left(\frac{M_\infty}{Re}\right)^2 C_2\frac{P_k}{k} \quad (4)$$

The time and length scales are computed as

$$T'=\max\left[\frac{k}{\epsilon},6\sqrt{\frac{\nu}{\epsilon}}\right]\ ,\ \ T=\min\left(T',\left(\frac{Re}{M_\infty}\right)\frac{\alpha k}{\sqrt{3}C_\mu\overline{v^2}\sqrt{2S_{ij}S_{ij}}}\right)$$

$$L' = \min\left(\frac{k^{3/2}}{\epsilon}, \left(\frac{Re}{M_\infty}\right)\frac{k^{3/2}}{\sqrt{3}C_\mu\overline{v^2}\sqrt{2S_{ij}S_{ij}}}\right), \quad L = C_L \max\left[L', C_\eta(\frac{\nu^3}{\epsilon})^{1/4}\right]$$

where $S_{ij} = 0.5(\partial u_i/\partial x_j + \partial u_j/\partial x_i)$ represents the strain tensor. The upper bound for the time and length scales is derived from realizability constraints (Durbin 1996). The eddy-viscosity is given by

$$\mu_t = C_\mu \overline{v^2} T,$$

and the model constants are:

$$C_\mu = 0.19,\ \sigma_k = 1,\ \sigma_\epsilon = 1.3,\ C_{\epsilon 1} = 1.4(1 + 0.045\sqrt{k/\overline{v^2}}),\ C_{\epsilon 2} = 1.9,$$

$$C_1 = 1.4,\ C_2 = 0.3,\ C_L = 0.3,\ C_\eta = 70,\ \alpha = 0.6.$$

The wall boundary conditions for ϵ and f are derived from the near wall asymptotic behavior of the k and $\overline{v^2}$ equations forcing $k \sim y^2$ and $\overline{v^2} \sim y^4$,respectively, as $y \to 0$.

$$k_w = 0,\ \overline{v_w^2} = 0,\ \epsilon_w = \left(\frac{M_\infty}{Re}\right)^2 \frac{2\nu k_1}{y_1^2},\ f_w = -\left(\frac{M_\infty}{Re}\right)^4 \frac{20\nu^2\overline{v_1^2}}{\epsilon_w y_1^4} \tag{5}$$

The indices w and 1 denote respectively the wall and first point above the wall.

2.3 Numerical solution of the turbulence equations

CFL3D uses a segregated approach for the solution of the mean flow and turbulence equations. This facilitates the implementation of the v^2-f model such that the turbulence model can be solved in a single subroutine. Only the boundary conditions are set up elsewhere.

The k, ϵ and $\overline{v^2}$, f equations are solved in a pairwise coupled manor similarly to the implementation in INS2D (Durbin 1995). An equation-by-equation approach used, for example, in STREAM (Lien *et al.* 1996) does not allow an implicit coupled treatment of the boundary conditions. This has been observed to cause convergence problems and may require the use of smaller time steps. In this report we consider only the implementation of the $\overline{v^2}$ and f equations. The k and ϵ equations are discretized and solved in a similar fashion. Equations (3) and (4) written for an implicit scheme in delta form are:

$$\left(I(\frac{1}{\Delta t} + \left(\frac{Re}{M_\infty}\right)\frac{\epsilon}{k}) + \delta_\eta A_\eta + \delta_\xi A_\xi + \delta_\zeta A_\zeta\right)\Delta\overline{v^2} - \left(\frac{Re}{M_\infty}\right)k\Delta f = R \tag{6}$$

with

$$R = -(\delta_\eta A_\eta + \delta_\xi A_\xi + \delta_\zeta A_\zeta)\overline{v^2}^n + \left(\frac{Re}{M_\infty}\right)kf^n - \left(\frac{Re}{M_\infty}\right)\frac{\epsilon}{k}\overline{v^2}^n$$

and

$$(I + \delta_\eta B_\eta + \delta_\xi B_\xi + \delta_\zeta B_\zeta)\Delta f = Q \tag{7}$$

with

$$Q = -L^2(\delta_\eta B_\eta + \delta_\xi B_\xi + \delta_\zeta B_\zeta)f^n - f^n + \frac{C_1}{T}\left[\frac{2}{3} - \frac{\overline{v^2}^n}{k}\right] + \left(\frac{M_\infty}{Re}\right)^2 C_2 \frac{P_k}{k}$$

Here $\delta_\xi A_\xi$ and $\delta_\xi B_\xi$ (in analogy η and ζ) define the expressions

$$\delta_\xi A_\xi = \delta_\xi U_\xi - \left(\frac{M_\infty}{Re}\right)\frac{1}{\rho}\delta_\xi[(\mu + \frac{\mu_t}{\sigma_k})\delta_\xi] \ , \ \delta_\xi B_\xi = -\left(\frac{M_\infty}{Re}\right)^2 \delta_\xi^2$$

The variables $k, \epsilon, \mu_t, L, T, \rho$, and U are set at their previously computed values and thus treated as constant in time. The time update is defined as

$$\Delta\overline{v^2} = \overline{v^2}^{n+1} - \overline{v^2}^n \ , \ \Delta f = f^{n+1} - f^n$$

As mentioned, the wall boundary conditions are treated implicitly. As usual in a cell centered scheme, two rows of halo, or ghost, cells are added to the computational domain. The values in the first row of halo cells are denoted by subscript 0. The values at wall boundaries are linearly extrapolated from the interior. In delta form the equations are:

$$\Delta k_0 = -\Delta k_1, \ \Delta\overline{v_0^2} = -\Delta\overline{v_1^2}, \ \Delta\epsilon_0 = 2\Delta\epsilon_w r - \Delta\epsilon_1, \ \Delta f_0 = 2\Delta f_w r - \Delta f_1 \qquad (8)$$

It has been found that particularly at the beginning of a calculation very small time steps are required to prevent k and $\overline{v^2}$ from becoming negative, which often leads to divergence of the solution. Particularly the value of ϵ at the wall is initially very large due to the factor $1/y^2$ in the boundary condition. The wall distance of the first cell center above the wall y_1 is usually of the order of 10^{-6} times the airfoils cord. Keeping the dissipation of the turbulent kinetic energy ϵ small at the wall during the first iterations ensures a rapid growth of the turbulent kinetic energy and thus of the turbulent boundary layer. One way to relax the ϵ and f boundary conditions can be achieved by multiplying their wall values by a factor which is dependent on the iteration counter n

$$r = \frac{\min(n, n_a)}{n_a}$$

Here n_a is the iteration number up to which the boundary condition is modified. For most applications it has been set to 100.

The convective terms in the k, ϵ, and $\overline{v^2}$ transport equations have been discretized as first-order upwind differences. This increases robustness, and usually this is sufficiently accurate for the turbulence equations since the source terms mainly balance the diffusion terms in wall bounded flows.

The time and length scales require an upper bound only in fully turbulent calculations with stagnation regions to suppress the spurious production of eddy-viscosity (Durbin 1996). However, the strain magnitude S is particularly large close to the wall at the initial iterations. This oversuppresses the value of the eddy-viscosity, hindering the development of a turbulent boundary layer. Therefore fully turbulent flow has been computed without an upper limit on the time and length scales for the first 100 or so iterations.

2.4 Transition modeling

Particularly for high lift computations it can be very important to model transition. Transition is modeled in a crude way by switching off the production source terms in the laminar part of the flow upstream of an a priorly fixed transition line. It has been found that solely switching off the terms which include P_k upstream of transition leads often to numerical difficulties. Large residuals caused by negative values of the turbulent variables prevent convergence in this region. Limiting the lower value of the turbulent variables with the free-stream values and additionally setting f to 0 at the walls upstream of transition seems to eliminate this problem.

The stagnation point anomaly usually does not appear for airfoil computations with a priorly fixed transition. No upper bounds on the time and length scales are therefore needed.

2.5 Approximate Factorization

In the 2-D flow solver INS2D, the matrices on the left-hand side in (6) and (7) are ILU-preconditioned and subsequently solved with the Generalized Minimum Residual (GMRES) (Saad 1986) algorithm. For 3-D computations the non-zero band width in the sparse matrices increases significantly with the third dimension. The inversion of these matrices with GMRES is not practical in the computation of industrial flows due to the large amount of memory required.

A three-factored Approximate Factorization scheme, as used for the mean flow, factorizes our system of Eqs. (6) and (7) into three 1-D problems:

$$\left(I(1+\left(\frac{Re}{M_\infty}\right)\frac{\epsilon}{k}\Delta t)+\delta_\eta A_\eta \Delta t\right)\Delta\overline{v^2}' - \left(\frac{Re}{M_\infty}\right)k\Delta t\Delta f' = R\Delta t \tag{9}$$

$$(I+\delta_\eta B_\eta \alpha)\Delta f' = Q\alpha$$

along η grid lines,

$$(I+\delta_\xi A_\xi \Delta t)\Delta\overline{v^2}'' = \Delta\overline{v^2}' \tag{10}$$

$$(I+\delta_\xi B_\xi \alpha)\Delta f'' = \Delta f'$$

along ξ grid lines, and

$$(I+\delta_\zeta A_\zeta \Delta t)\Delta\overline{v^2}''' = \Delta\overline{v^2}'' \tag{11}$$

$$(I+\delta_\zeta B_\zeta \alpha)\Delta f''' = \Delta f''$$

along ζ grid lines. A modification of the elliptic relaxation equation is required to factorize the matrices. Here the term Δf on the left-hand side in (7) has been substituted with an unsteady like term $\Delta f/\alpha$.

The error of this scheme can be estimated by substituting $\Delta\overline{v^2}''$, $\Delta\overline{v^2}'$, $\Delta f''$ and $\Delta f'$ with the expressions (10) and (11):

$$\left(I(1+\left(\frac{Re}{M_\infty}\right)\frac{\epsilon}{k}\Delta t)+(\delta_\eta A_\eta+\delta_\xi A_\xi+\delta_\zeta A_\zeta)\Delta t\right)\Delta\overline{v^2}''' - \left(\frac{Re}{M_\infty}\right)k\Delta t\Delta f'''$$

$$+\underline{\left(I\left(\frac{Re}{M_\infty}\right)\frac{\epsilon}{k}(\delta_\xi A_\xi+\delta_\zeta A_\zeta)+\delta_\eta A_\eta\delta_\xi A_\xi+\delta_\eta A_\eta\delta_\zeta A_\zeta+\delta_\xi A_\xi\delta_\zeta A_\zeta\right)\Delta t^2\Delta\overline{v^2}'''}$$

$$-\underline{\left(\frac{Re}{M_\infty}\right)k(\delta_\xi B_\xi+\delta_\zeta B_\zeta)\Delta t\alpha\Delta f'''+\left(I\left(\frac{Re}{M_\infty}\right)\frac{\epsilon}{k}+\delta_\eta A_\eta\right)\delta_\xi A_\xi\delta_\zeta A_\zeta\Delta t^3\Delta\overline{v^2}'''}$$

$$-\underline{\left(\frac{Re}{M_\infty}\right)k\delta_\xi B_\xi\delta_\zeta B_\zeta\Delta t\alpha^2\Delta f'''}=R\Delta t \tag{12}$$

$$\left(I+(\delta_\eta B_\eta+\delta_\xi B_\xi+\delta_\zeta B_\zeta)\alpha\right)\Delta f'''+\underline{\left(\delta_\eta B_\eta\delta_\xi B_\xi+\delta_\eta B_\eta\delta_\zeta B_\zeta+\delta_\xi B_\xi\delta_\zeta B_\zeta\right)\alpha^2\Delta f'''}$$

$$+\underline{\delta_\eta B_\eta\delta_\xi B_\xi\delta_\zeta B_\zeta\alpha^3\Delta f'''}=Q\alpha \tag{13}$$

The terms underlined are error terms which modify the original Eqs. (6) and (7). They are, however, scaled by powers of the time step Δt and the variable α. Small values of α and Δt minimize the influence of these error terms. On the other hand, a small α modifies the f equation significantly, which is represented exactly in the non-underlined part of Eq. (13), setting $\alpha = 1$. A local time step is used for steady state computations. The time step Δt for transonic flow around the RAE 2822 airfoil (Cook *et al.* 1979) is, for example, of the order of 10^{-5} near the wall, 0.1 at the edge of the boundary layer, and 10 in the free-stream. A constant value of α between 0.1 and 0.01 has been found to work quite well. Note that at convergence Eq. (13) becomes

$$Q = 0$$

and the exact f-equation is solved, irrespective of α.

The matrices on the left-hand side of (9), (10), and (11) are tridiagonal 2×2 block matrices. A direct solver taken from a 1-D channel code is used to invert these matrices. Sub-iterations for the turbulence model could be used to correct the approximation errors (Steinthorsen *et al.* 1993). However, the test cases run so far have been computed without the use of sub-iterations.

It should be noted that the source terms are treated implicitly only with the first factorized matrix (cf. Eq. (9)). The $''$ and $'''$ time updates in the first cell above the wall do not 'see' the wall and are treated in the same way as in the internal cells. The boundary condition is thus applied only to the first update $'$ and not to the final update $'''$. This allows only certain grid lines, here the η-lines, to be normal to a wall, severely limiting the usability of the three-factored scheme. Nevertheless, several airfoil computations and the 3-D ONERA M6 wing computation described later in this report have been successfully carried out with this approach.

Furthermore, it should be noted that only a 1-D array with twice the largest grid dimension ('twice' since two equations are solved simultaneously) is required for the factorization procedure described. However, consistent with other turbulence models implemented in CFL3D, 2-D arrays have been employed, improving the vectorization of the direct solver and reducing the number of operations. These 2-D arrays are first filled in the $\xi - \eta$ plane with the 1-D operator in η direction, then with the 1-D operator in ξ direction, and finally in the $\xi - \zeta$ plane with the 1-D operator in ζ direction.

A two-factored Approximate Factorization scheme overcomes some of the difficulties described. Instead of factorizing the original 3-D system of equations into three 1-D system of equations, the two-factored scheme solves a 2-D and 1-D set of equations:

$$\left(I(1+\left(\frac{Re}{M_\infty}\right)\frac{\epsilon}{k}\Delta t)+\delta_\eta A_\eta \Delta t+\delta_\xi A_\xi \Delta t\right)\Delta\overline{v^2}'-\left(\frac{Re}{M_\infty}\right)k\Delta t\Delta f'=R\Delta t \quad (14)$$

$$(I+\delta_\eta B_\eta \alpha+\delta_\xi B_\xi \alpha)\Delta f'=Q\alpha$$

in the $\xi-\eta$ plane and

$$(I+\delta_\zeta A_\zeta \Delta t)\Delta\overline{v^2}''=\Delta\overline{v^2}' \quad (15)$$

$$(I+\delta_\zeta B_\zeta \alpha)\Delta f''=\Delta f'$$

along ζ grid lines. Practically only the diagonals of the operators $\delta_\eta A_\eta$, $\delta_\xi A_\xi$ and $\delta_\eta B_\eta$, $\delta_\xi B_\xi$ have to be added, allowing the use of the same 2-D arrays. Solving the resulting 2-D matrix with GMRES the implicit source terms are included in the η direction as well as in the ξ direction. These can now be normal to the walls.

The approximation errors of this scheme follow by substituting $\Delta\overline{v^2}'$ and f' with the expressions of (15)

$$\left(I(1+\left(\frac{Re}{M_\infty}\right)\frac{\epsilon}{k}\Delta t)+(\delta_\eta A_\eta+\delta_\xi A_\xi+\delta_\zeta A_\zeta)\Delta t\right)\Delta\overline{v^2}''-\left(\frac{Re}{M_\infty}\right)k\Delta t\Delta f'' \quad (16)$$

$$\underline{+(I\left(\frac{Re}{M_\infty}\right)\frac{\epsilon}{k}+\delta_\eta A_\eta+\delta_\xi A_\xi)\delta_\zeta A_\zeta \Delta t^2\Delta\overline{v^2}''-\left(\frac{Re}{M_\infty}\right)k\delta_\zeta B_\zeta \Delta t\alpha\Delta f''=R\Delta t}$$

$$(I+\delta_\eta B_\eta \alpha+\delta_\xi B_\xi \alpha+\delta_\zeta B_\zeta \alpha)\Delta f''+\underline{(\delta_\eta B_\eta+\delta_\xi B_\xi)\delta_\zeta B_\zeta \Delta f''\alpha^2}=Q\alpha \quad (17)$$

Again we have underlined the error terms. The number of these terms is substantially smaller than when using the three-factored scheme. Additionally, these terms scale with Δt^2 (or with α^2) as opposed to the three-factored scheme, the error of which scale with Δt^3 (or α^3). Often larger time steps can be used. For some flows such as the transonic flow around the RAE 2822 airfoil under the flow conditions of test case 10 (Lien *et al.* 1998), the computation with the v^2-f model and the three-factored scheme did not converge. It had to be computed using GMRES.

The memory requirements for the three-factored and two-factored scheme described are almost the same in CFL3D. They are far smaller than for a procedure in which the original 3-D system of equations is inverted with GMRES.

Currently, all memory additionally required for GMRES is provided locally. Some of the computer operations could be optimized by reordering the coding. The scaling of the f equation with Re/M_∞ affects the eigenvalues of the implicit matrices. This influences the number of GMRES sub-iterations required as well as the convergence tolerance used. 10 GMRES subiterations with a convergence tolerance of 10^{-8} is currently used and may still be optimized in future research.

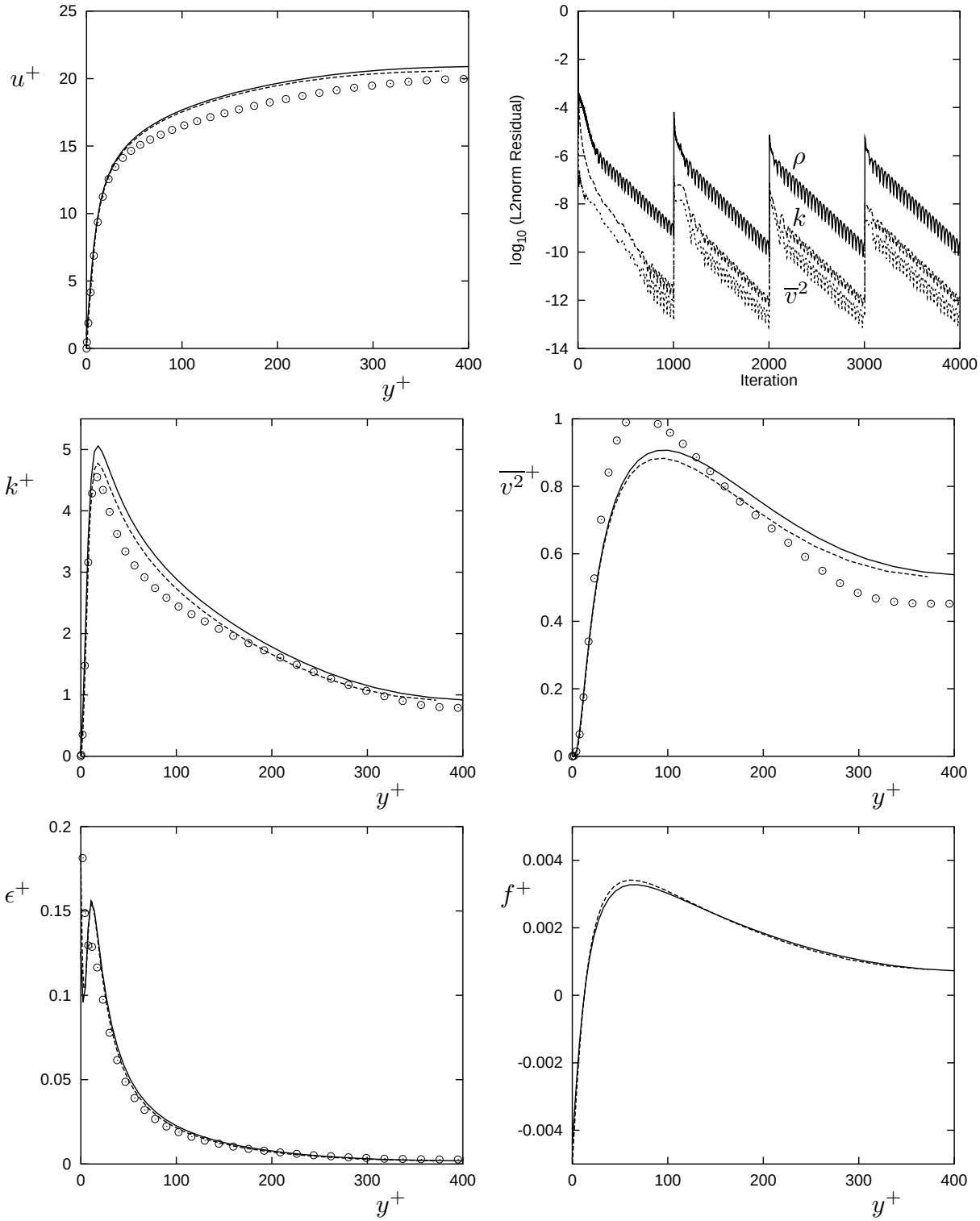

FIGURE 1. Profiles for channel flow, $Re_{u_\tau} = 395$; ——— : v^2-f model and CFL3D, - - - - :v^2-f model and 1-D channel code, ∘ : DNS.

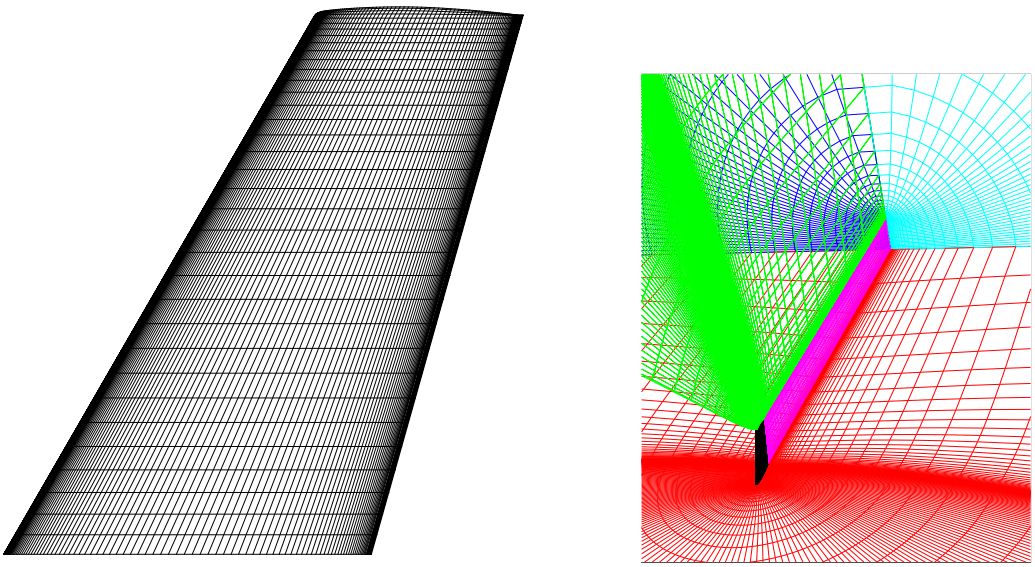

FIGURE 2. Surface mesh and C-O mesh structure for ONERA M6 wing.

2.6 Channel flow

Channel flow has been computed to validate the correctness of the v^2-f implementation in CFL3D. DNS data exists for incompressible flow for $Re_{u_\tau} = 395$ based on the wall shear velocity u_τ and the channel half-width h. A Mach number of $M = 0.2$ has been specified for the computation with CFL3D.

Periodic boundary conditions as for incompressible channel flow can not be specified since the friction at the wall leads to an entropy production which increases the flow temperature. A very long channel $h = 1m, l = 50m$ (32×96 cells) has therefore been computed, avoiding code modifications. The height of the first cell above the wall is 5×10^{-3}, corresponding to a cell-centered value of $y^+ = 1$.

The pressure is extrapolated and the other flow parameters are specified at the inflow of the channel. The pressure at the outflow is obtained over the total enthalpy, which remains constant in the flow for adiabatic walls. The outflow data is then copied to the inflow after achieving convergence. This procedure is repeated until periodicity is obtained with a good approximation, indicating fully developed channel flow. A Reynolds number of about $Re = 7500$, based on the mean flow velocity and the channel half-width h, has been found iteratively to correspond to the correct wall shear velocity.

The convergence plots are given in Fig. 1, which shows the restarted solutions. In the same figure profiles of the velocity and turbulent quantities are plotted against the wall distance y^+. The data computed with CFL3D corresponds quite well with data computed with an incompressible 1-D channel code.

2.7 ONERA M6 wing.

Flow over the ONERA M6 wing (Schmidt *et al.* 1970) has been computed for the flow conditions: Mach number $M = 0.8395$, Reynolds number $Re_c = 11.72 \times 10^6$

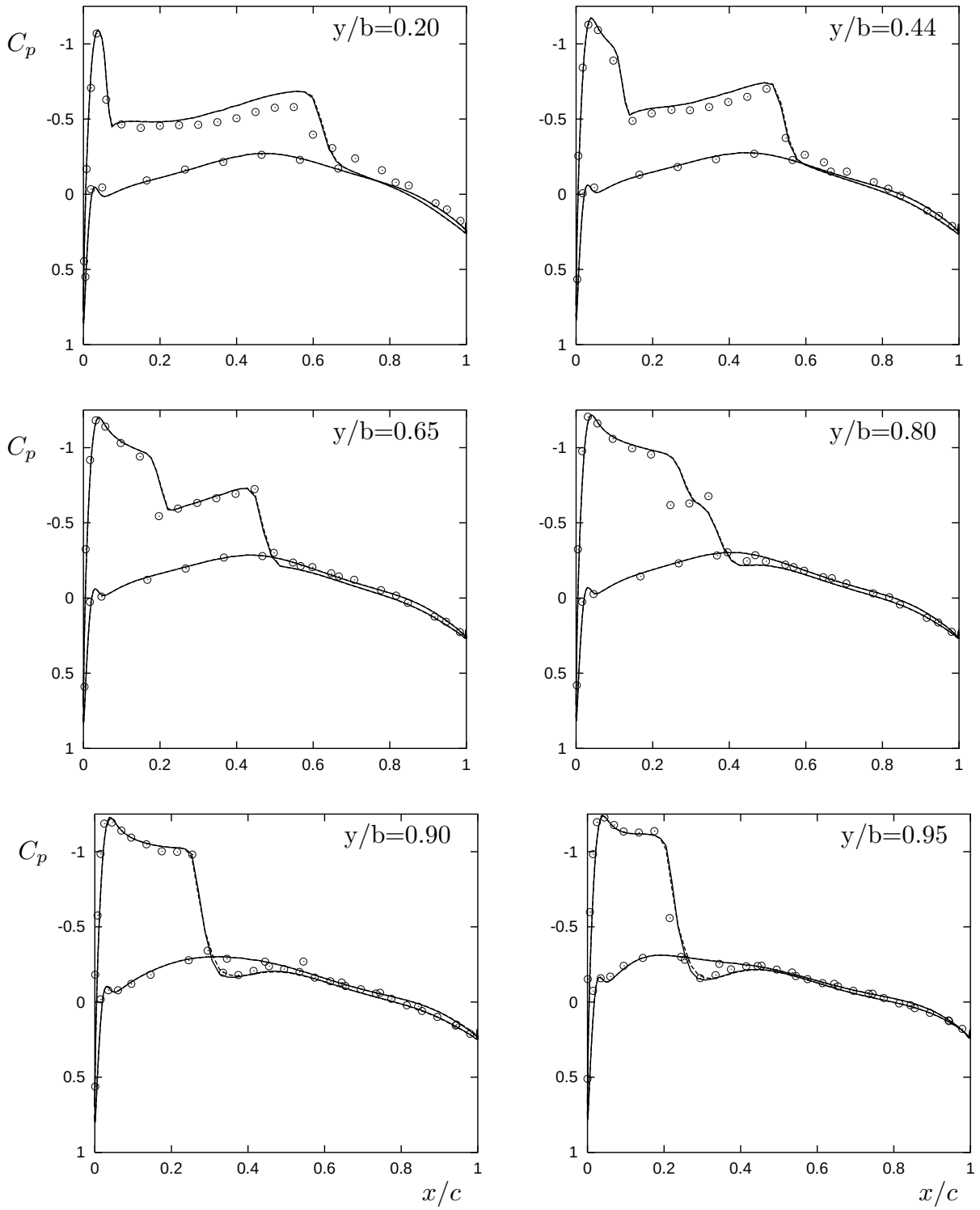

FIGURE 3. Pressure coefficient at cuts for ONERA M6 wing; ——— : v^2-f model, - - - - : Spalart-Allmaras, ∘ : Experiment.

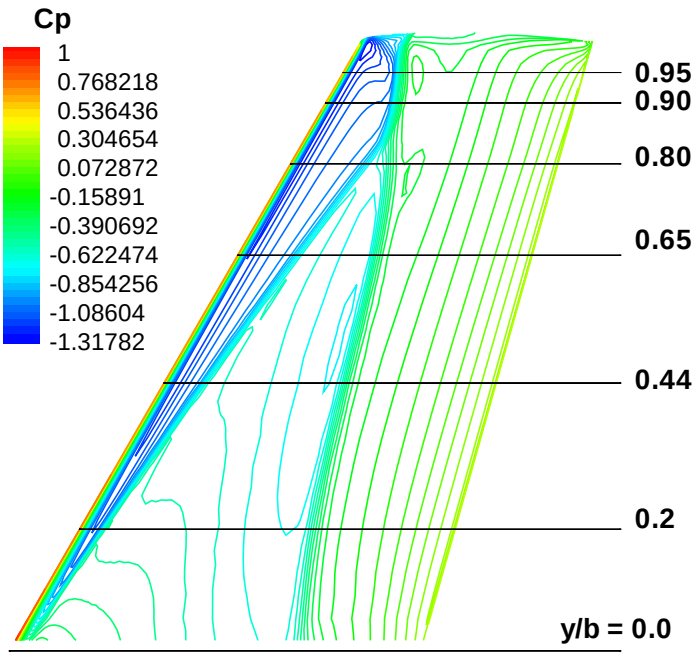

FIGURE 4. Pressure coefficient distribution on ONERA M6 wing (cell-centered data), v^2-f model.

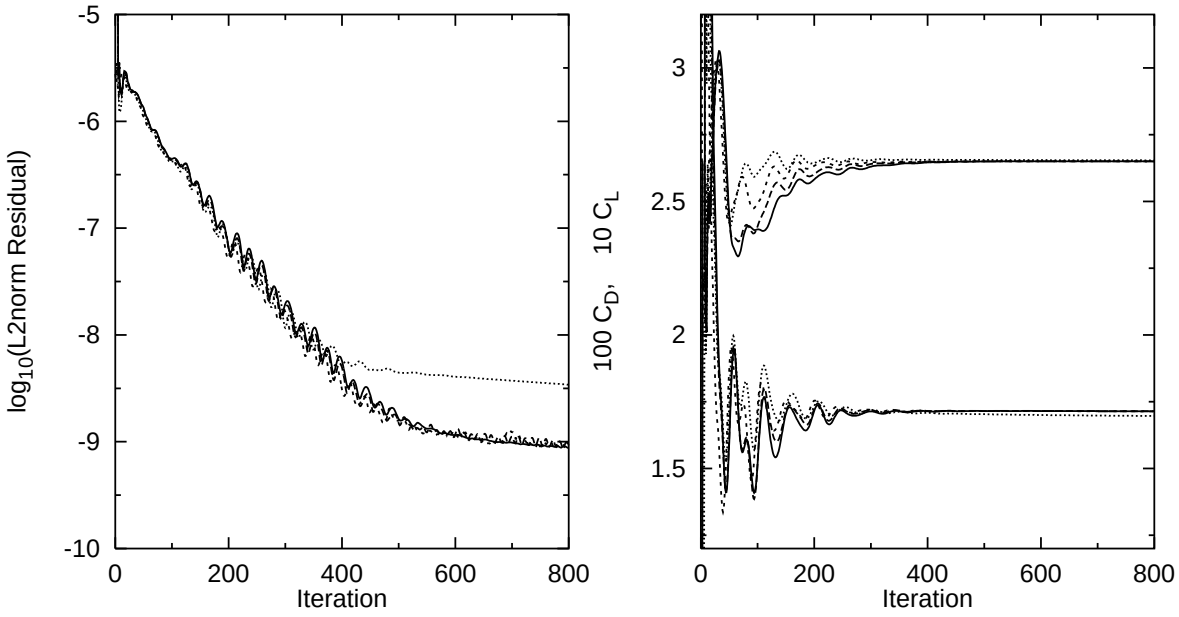

FIGURE 5. Lift, drag and density convergence for ONERA M6 wing; ——— : v^2-f and three-factored AF, – – – : v^2-f and two-factored AF/GMRES, - - - - : v^2-f and GMRES, ····· : Spalart-Allmaras.

based on the mean chord of $c = 0.64607$ and incidence $\alpha = 3.06^o$. This is a swept wing with a root chord of about $c_{root} = 0.8m$ and a span of about $b = 1.2m$. The airfoil profile is symmetric.

The computational grid has been generated with the HYPGEN software package provided by P. Buning (see Chan *et al.* 1993). The single block C-O mesh consists of 665 856 cells (696 969 nodes) with 272 cells in the streamwise direction, 68 normal to the wall, and 36 in the spanwise direction. The inflow is located about 15 chord lengths into the far field. The surface mesh on the wing is 100×36 cells on both the upper and lower surfaces. A plan view of the surface mesh is shown together with the general C-O mesh structure in Fig. 2.

A comparison of pressure distributions computed with the v^2-f and Spalart-Allmaras model with experimental data at selected wing cuts is shown in Fig. 3. The corresponding pressure distribution on the upper wing surface and the location of the cuts are shown in Fig. 4. Although a generally good agreement of the computed and the experimental data can be observed, the pressure distribution at station $y/b = 0.80$ shows both branches of the shock merging prematurely. The pressure distribution on the wing depends more on the particular numerical scheme (i.e. the flux limiter chosen) than the turbulence model used.

The plots in Fig. 5 show a similar convergence history for both models. All three numerical schemes work well for the v^2-f model for this test case. The computations have been carried out with local time steps corresponding to a CFL number of 5.

The computational cost for 800 iterations on a CRAY C90 with the v^2-f model is about 3.1 CPU hours using 42.3 Mword memory with the three-factored scheme and 4.9 hours using 43.6 Mword with the two-factored scheme, in which GMRES has been used in a plane containing the wall normal and streamwise direction. For the solution of the original 3-D problem with GMRES, the CPU time is 12.0 hours using 126.0 Mword memory. For the Spalart-Allmaras model 2.3 CPU hours are required with 38.2 Mword memory.

3. Summary and future plans

The present report describes the current implementation of the v^2-f model in the compressible 3-D flow solver CFL3D. Both an Approximate Factorization scheme and the Generalized Minimum Residual algorithm are implemented for the solution of the turbulence equations. The stiff boundary condition for ϵ and f require that both the source terms and the boundary conditions are treated implicitly in the wall normal direction. This restricts the very fast and memory efficient three-factored Approximate Factorization scheme to computations in which grid lines of the same coordinate, for example η, are normal to the wall. The two-factored scheme allows grid lines of two coordinate directions to be normal to the wall using the same memory requirements. This increases the applicability of the v^2-f model in large flow computations around complex geometries. While less efficient regarding the CPU time needed per iteration, it often permits the use of larger time steps.

The report provides a comparison of a three-factored, a two-factored, and a GMRES solution of the original 3-D turbulence equations. The efficiency of each scheme is demonstrated on the computation of transonic flow around the ONERA M6 wing.

Although all three schemes perform similarly for this test case in terms of convergence per iteration, they require different CPU time and computer memory. The two-factored scheme requires 1.6 times the CPU time of the three factored scheme, using about the same computer memory. The full GMRES solution requires about 2.9 times the amount of memory of both other schemes and 3.9 times the CPU time of the three-factored scheme. However, as mentioned, the implementation of the GMRES routines may not be optimal and can be improved further through future work.

The Spalart-Allmaras model, which consists of one transport equation as opposed to the v^2-f's four partial differential equations, requires 0.74 times the CPU time and 0.90 times the computer memory of the v^2-f computation with the three-factored scheme.

An unsteady term has been added to the f-equation in order to use the Approximate Factorization scheme. Subiterations may be needed to minimize the influence of this term in unsteady computations.

Computation of high-lift test cases are underway which depend significantly on the turbulence model used. Here we concentrate on the computation of flow around the three element trapezoidal wing-body currently investigated experimentally in the wind tunnel at NASA Langley. A patched mesh consisting of about 8 million grid points has been provided by the Subsonic Aerodynamics Branch at Langley (Jones *et al.* 1998).

Computations of the two element NLR7301 airfoil (Van den Berg 1979) and the McDonnell-Douglas slat-wing-flap airfoil (Valarezo *et al.* 1991), previously computed with the INS2D code (Kalitzin 1997), with use of patched and chimera grids is planned. In addition boundary conditions for the ϵ and f equations in flow regions such as the blunt trailing edge of an airfoil may require modifications.

As reported in the CTR Summer Program (Lien, *et al.* 1998), some of the airfoil computations required the use of constant time steps for the integration of the turbulence equations. Small unsteady oscillations in $\overline{v^2}$ and f prevented the solutions from converging using local time steps. This is another aspect for future research.

It is also planned to have a closer look at the shock-boundary layer interaction region, for example for the RAE 2822 test cases. The sonic line parallel to the wall lies deep inside the boundary layer. As pointed out by Bradshaw (1998), the true domain of dependence of a point just upstream of the shock wave is the upstream Mach cone, which blends into the sonic line, plus the subsonic region near the wall. The integration of the f-equation over the whole domain, including shock and the region behind it, introduces errors in comparison to an integration of the f-equation over the upstream-and-subsonic domain only. This research should estimate the significance of this error.

REFERENCES

Van den Berg, B. 1979 Boundary layer measurements on a two-dimensional wing with flap. *NLR TR 79009 U.*

Beam R. M., & Warming R. F. 1978 An implicit factored scheme for the compressible Navier-Stokes equations. *AIAA J.* **16,** 393-402.

Bradshaw, P. 1998 private communications.

Chan, M. W., Chiu I.-T. & Buning, P. G. 1993 User's manual for the HYPGEN hyperbolic grid generator and the HGUI graphical user interface. *NASA TM 108791.*

Cook, P. H., McDonald, M. A. & Firmin, M. C. P. 1979 Aerofoil 2822 - Pressure Distributions, Boundary Layer and Wake Measurements. *AGARD AR 138.*

Durbin, P. 1995 Separated flow computations with the $k-\epsilon-\overline{v^2}$ model. *AIAA J.* **33,** 659-664.

Durbin, P. 1996 On the k-ϵ stagnation point anomaly. *Int. J. Heat and Fluid Flow.* **17,** 89-90.

Jones, K. & Compton, W. B. 1998 private communications.

Kalitzin, G. 1997 Application of turbulence models to high-lift airfoils. *CTR Annual Research Briefs.* Center for Turbulence Research, NASA Ames/Stanford Univ., 165-177.

Krist, S., Biedron, R. & Rumsey, C. 1998 CFL3D User's Manual (Version 5.0). *NASA/TM-1998-208444.*

Lien F. S. & Durbin P. A. 1996 Non-linear $k-\epsilon-v^2$ modeling with application to high-lift. *CTR Summer Program Proceedings.* Center for Turbulence Research, NASA Ames/Stanford Univ., 5-22.

Lien F. S., Kalitzin G. & Durbin P. A. 1998 RANS modeling for compressible and transitional flows. *CTR Summer Program Proceedings.* Center for Turbulence Research, NASA Ames/Stanford Univ., 267-286.

Saad, Y. & Schultz M. H. 1986 GMRES: a generalized minimal residual algorithm for solving nonsymmetric linear systems. *SIAM J. Sci. Stat. Comp.* **7,** 856-869.

Schmitt, V. & Charpin F. 1970 Pressure distribution on the ONERA M6 wing at Transonic Mach Numbers. *AGARD AR138: Experimental Database for computer program assessment.*

Spalart, P. R. & Allmaras, S. R. 1992 A one-equation turbulence model for aerodynamic flows. *AIAA 92-439.*

Steinthorsen, E. & Shih, T.I-P. 1993 Methods for Reducing Approximate-Factorization Errors in Two- and Three-Factored Schemes. *SIAM J. Sci. Comput.* **14-3,** 1214-1236.

Valarezo, W. O., Dominik, C. J., McGhee, R. J., Goodman, W. L. & Paschal, K. B. 1991 Multi-Element Airfoil Optimization for Maximum Lift at High Reynolds Numbers. *AIAA 91-3332.*